Quantum Interference in Fully Depleted Tri-Gate Quantum-Wire Transistors—The Role of Inelastic Scattering

Matthew J. Gilbert, *Student Member, IEEE,* and David K. Ferry, *Fellow, IEEE*

***Abstract*—Within the next decade, it is predicted that we will reach the limits of silicon scaling as it is currently defined. Of the new devices under investigation, one of the most promising is the tri-gate quantum-wire transistor. In this paper, we study the role quantum interference plays in the operation of this device both in the ballistic and quasi-ballistic regimes. We find that, in the ballistic case, the electrons propagating in the system tend to form vortices in their motion when subjected to moderate drain biases. These vortices form in both the source and drain of the device when the proper conditions are satisfied. Further, we observe fluctuations in the conductance of the device, which leads to fluctuations in resultant drain current due to interactions with the channel and dopant ions. When inelastic scattering is considered, the formation of the vortices is suppressed and the spread in threshold voltage fluctuations is reduced. However, the conductance fluctuations remain in the drain current once the drain voltage reaches larger values.**

***Index Terms*—Inelastic scattering, MOSFET, quantum interference, quantum wire, silicon, tri-gate, vorticity.**

I. Introduction

FOR MANY years, the semiconductor industry has been quite successful at scaling current CMOS technology to fit the growing demands. Nevertheless, when we look beyond 2010, there is some question as to what will be the next transistor technology. While progress on the MOSFET has been quite steady, tri-gate technology is thought to offer better performance over traditional silicon technology and to have better scaling possibilities and easier fabrication using conventional processing tools and techniques [1]. On the other hand, it is possible to fabricate MOS devices in a silicon-on-insulator (SOI) environment with channel widths as small as 2 nm [2]. These devices are clearly quantized in all three directions and must be treated as such without resorting to the separation of one or more dimensions in terms of basis expansions. In this paper, we study tri-gate SOI devices with a fully quantum mechanical three-dimensional (3-D) self-consistent device simulation tool based on the scattering matrix technique [3]. Here, we examine the effect of scattering on transport and current vortices in wide-channel ($\sim$18 nm) tri-gate devices.

II. Descirption of the Device and Model

The devices that we consider are tri-gate quantum-wire SOI MOSFETs. In general, the source and drain regions are a doped 6×10^{19} cm^{-3} n type. The dimensions of the source and the drain are 18.47-nm wide, 10.32-nm long, and 6.51-nm high (integer multiples of the Si atom spacing) corresponding to the thickness of the silicon layer. The channel of our device is a p-type region 9.77 nm in length, which is left undoped. The channel region has dimensions identical to that of the source and drain dimensions. A uniform 1-nm oxide layer covers the top and sides of the device to isolate the gates from the semiconductor. Under the device is a 100-nm-thick oxide layer.

This device is studied using the simulation approach presented in [3]. However, the method previously assumed that the transport in the device was ballistic, therefore, we must now modify the approach to include inelastic scattering. This is accomplished through the modification of the Hamiltonian. We include inelastic scattering as phase randomization in the simulation by introducing an imaginary potential [4]. For a phase coherent time τ_ϕ, the original site energy becomes

$$V_{\mathrm{mod}}(i,j,k) = V_{\mathrm{site}}(i,j,k) - i\Sigma(i,j,k) \tag{1}$$

where

$$\Sigma = \frac{\hbar}{2\tau_\varphi} \tag{2}$$

is the self-energy, which appears in the Hamiltonian. The phase coherence time of an electron in silicon is a well-known experimental result and may then be entered into the simulation.

With the scattering introduced to the Hamiltonian, we now scan the silicon lattice to distribute dopant atoms to the various regions of the device using the method presented in [5]. Using this method, the silicon lattice is traversed and dopants are randomly distributed. The charges are then mapped back to the solution space mesh once the doping is complete. This does create a situation where the size of the mesh does impact the size of the dopants placed in the simulation. However, when the charges are mapped back to the simulation grid, the charge from each dopant is distributed on a spatially dependent basis, which minimizes this effect. A typical potential profile is shown in Fig. 1.

All simulations are performed at 300 K. A nonuniform adaptable mesh has been implemented to ensure that all of the applied biases are kept within the artificial band structure created by the discretization of the Schrödinger equation. This ensures the physics is correct, while conserving grid points and the computation time. The adaptable mesh is not utilized when sweeps of the gate voltage are considered as the mesh required is close to uniform in all three dimensions. However, when the drain

Manuscript received August 11, 2004; revised March 11, 2005. This work was supported by the Office of Naval Research.

The authors are with the Department of Electrical Engineering, Arizona State University, Tempe, AZ 85287-5706 USA (e-mail: matthew.gilbert@asu.edu).

Digital Object Identifier 10.1109/TNANO.2005.851429

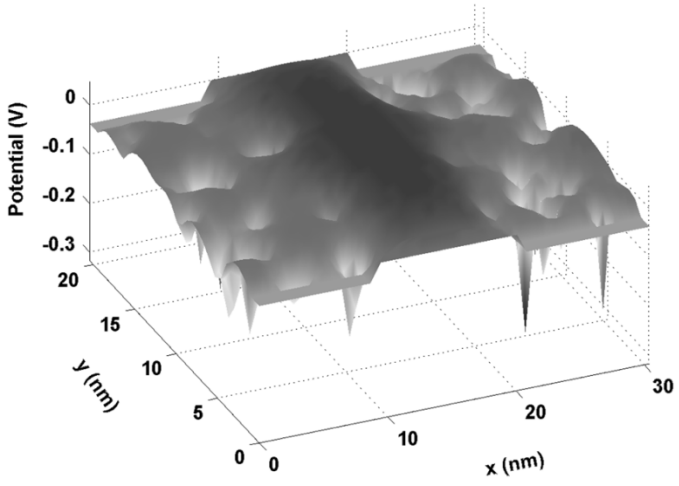

Fig. 1. Typical self-consistent potential profile for the quantum-wire tri-gate transistor under consideration in this paper. The localized donors in the source and drain form preferential sites in the potential.

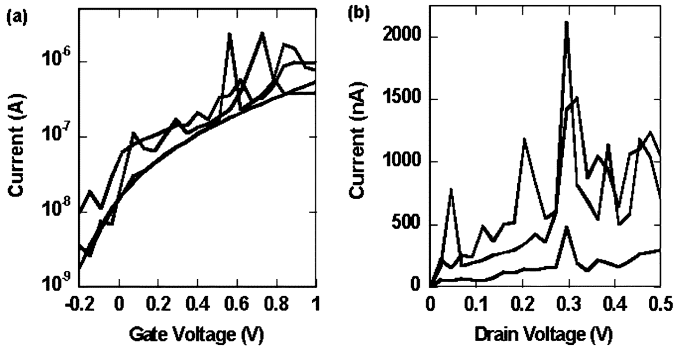

Fig. 2. (a) I_d–V_g curves for four different dopant distributions for $V_d = 100$ mV, where ballistic transport has been assumed. We see the results of the quantum interference, as well as threshold variations. The electron density interacting with the donors in the source and drain causes the observed spikes. (b) I_d–V_d curves corresponding to one tri-gate ballistic quantum-wire device. From bottom to top, the gate voltages are 0.1, 0.7, and 1.0 V. Again, large peaks are observed in the output current even at higher voltages.

voltage is swept, the mesh is highly nonuniform in all three dimensions. The simulations are not mesh dependent, as long as all of the relevant energies are kept within the artificial band-structure. Furthermore, the simulations are not energy integration dependent if the electron distribution where the transmission is taken varies slowly, as in a properly formed contact.

III. Results for the Ballistic Regime

A. I–V Characteristic

The I_d–V_g curves obtained from four different dopant distributions are shown in Fig. 1(a). The spikes present in the plots give an excellent example of the quantum interference effects that occur in this system. When the discreteness of the doping is taken into account, the landscape of the potential is drastically altered, as may be seen in Fig. 1. The potential dips now present in the source and drain set up additional reflections in the device, which add to the reflections already present in the device at the source–channel and channel–drain interfaces. These effects lead to the observance of the spikes in the curves shown in Fig. 1(a). The distribution of the dopants in the device has a profound effect on the *I–V* characteristics. The spikes in the current are much more pronounced in the devices that have donors distributed near the source–channel and channel–drain interfaces. In these devices, a resonant state may be formed in the channel at certain gate voltages, which leads to the form of the currents plotted in Fig. 2. We should note that, even in the absence of dopants in the channel, variations in the threshold voltage appear for different dopant configurations. This is a direct result of the quantum interference within the device. When we average over a ten-device sampling, we find the threshold voltage to be 0.113 V, but could vary by as much as 0.012 V in certain devices, where the threshold voltage is defined using the intercept method. While the concepts of dopant-induced fluctuations in the threshold voltage are not new, the fact that they are observed even in devices that have no channel doping has not been previously presented.

In Fig. 2(b), we examine drain voltage sweeps corresponding to only one distribution of donors. We find that, in general, the amplitude of the peaks in the drain current tend to increase as the gate voltage is increased. This can be explained by the fact that the gate voltage allows in more current carrying states, which interact with the source and drain dopants. The increased interaction causes the more pronounced interactions seen in Fig. 2(b). Nevertheless, while the interactions become greater as the gate voltage is increased, we find that the peaks still occur at the same value for the drain voltage. These effects are exacerbated due to the fact that the dimensions of these devices are small compared to the Fermi wavelength.

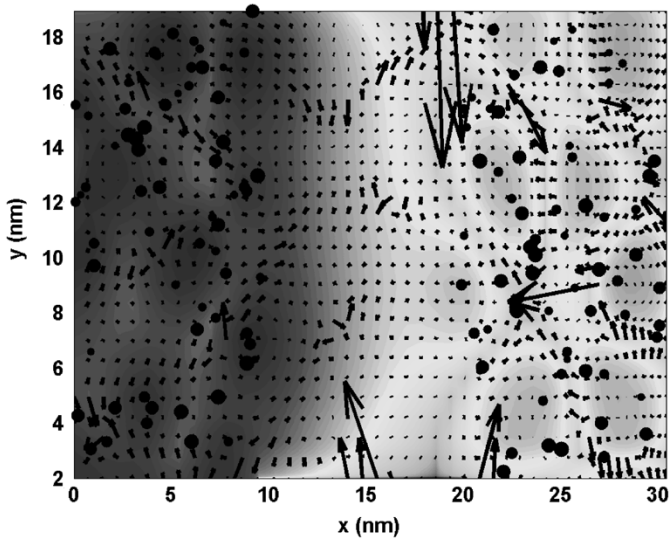

Fig. 3. Electron density at a depth of 7 nm into the device for $V_g = -0.05$ V and $V_d = 0.1$ V. Vortices form in the source and drain when dopant ions form a circular ring of potential at approximately the same depth.

B. Electron Density

In Fig. 3, we examine the electron density corresponding to a gate voltage of −0.05 V, which is below threshold. (Note that here and below we show only the source derived density in this figure.) The density and location of the dopant atoms are plotted and the corresponding velocity field pattern is then superimposed. The sizes of the dopant atoms in this figure show its relative position in the device. A dopant atom that is closer

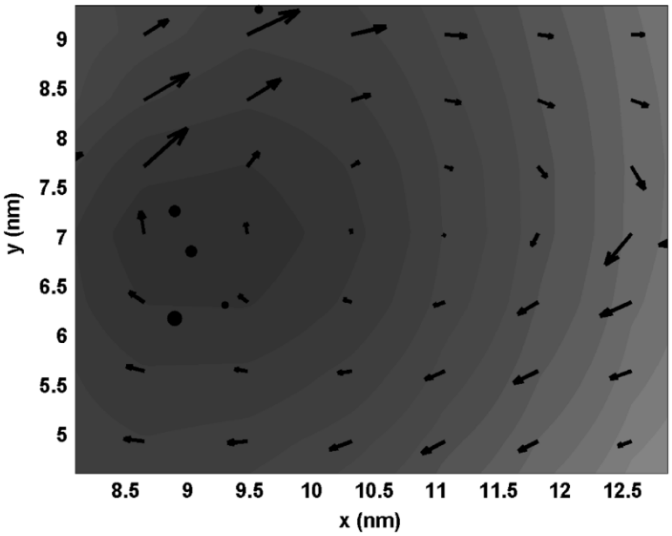

Fig. 4. Close-up of the vortex formed in the source of a tri-gate quantum-wire MOSFET device with $V_g = -0.05$ V and $V_d = 0.1$ V.

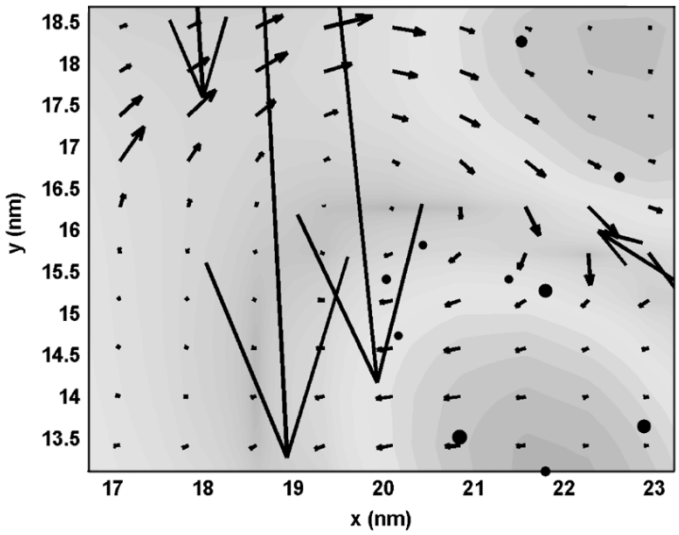

Fig. 5. Close-up of the vortex formed in the drain of a tri-gate quantum-wire MOSFET device with $V_g = -0.05$ V and $V_d = 0.1$ V.

to the surface of the device will appear larger than dopants that are buried deeper in the device. We plot only the positive propagating electron density so as to show the population of the channel and the filling of the drain states. While only the electron density corresponding to the positive propagating states is plotted, we consider both positive and negative propagating states when the self-consistent iteration is performed. The majority of the density in Fig. 3 is reflected at the source–channel interface. Nevertheless, some of the density is leaking into the channel. The density in the channel seems to have quite a regular flow pattern due to the fact that there are no dopant ions in the channel of the device to impede the flow. As the density leaks out of the channel into the drain, we see that it immediately begins to populate the donor sites. We see that the density is significantly lower at the channel–drain interface in all of the regions, except the region with the donor ions sitting on the edge of the interface. The fact that the electron density tends to coagulate in regions where the donor ions sit in the source and drain is due to the fact that the mapping of the charge back to the lattice creates energetically preferential sites where the electrons sit. It should be noted that the distribution of electrons to the energetically preferential sites is purely a result of the self-consistent calculation. Failure to reach convergence, or ignoring the correspondence between the classical and quantum potentials, not only results in inaccurate transmission, but also results in incorrect electron distributions. A calculation that lacks self-consistency would simply consist of lumps of density that would not correspond to the sites of the donors.

In Fig. 3, we find two vortices, one in the source and one in the drain. Close examination of these shows that they form when the donors are positioned in a circular pattern at approximately the same depth in the device [6], which corresponds to a totally different phenomenon than previously seen [7]. Here, we see dopant induced vortices in 3-D, whereas in [7], we have transport induced vortices. This is purely a 3-D effect. When this occurs, a ring of lower potential forms and the electron flow forms a vortex in the middle of these circularly distributed donors, as seen in Figs. 4 and 5.

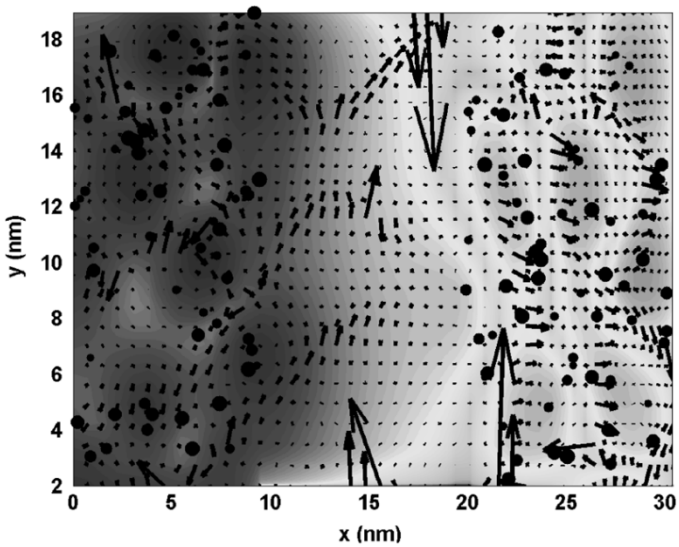

Fig. 6. Electron density at a depth of 7 nm into a tri-gate quantum-wire MOSFET device with $V_g = 0.35$ V and $V_d = 0.1$ V.

While this behavior occurs at gate voltages that are below threshold, it is natural to wonder if the same behavior persists at gate voltages above threshold. In Fig. 6, we plot the electron density for a gate voltage of 0.35 V, which is well above the threshold voltage. In this figure, the channel is now much more populated than is the earlier case. As the density leaves the preferential positions in the source, it once again spreads out into the undoped channel. Nevertheless, as it leaves the channel, we see that the density chooses to exit the channel into the nearest donor sites in the drain. We find that the drain vortex has now been washed away, but we do find two vortices in the source. The shape of the vortex in the top of the source (Fig. 7) remains the same as in Fig. 3, but the position of the vortex has shifted. Further, we find the formation of a second vortex in the bottom part of the source, shown in Fig. 8. These effects can be attributed to the change in the potential profile with the increase in the gate voltage.

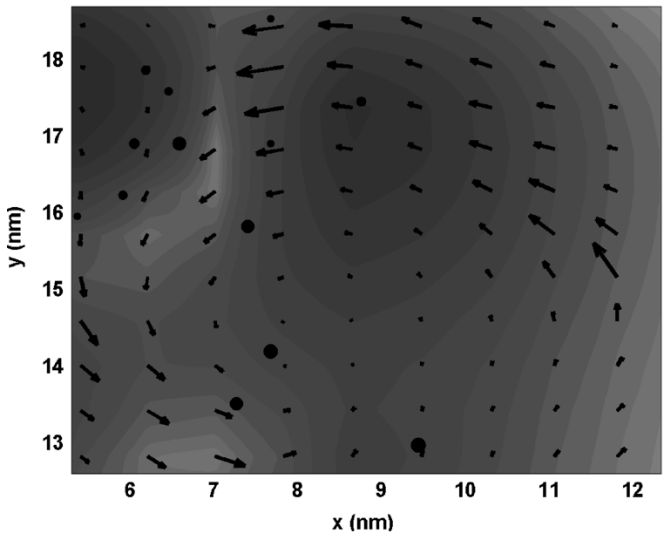

Fig. 7. Close-up of the vortex formed in the top of the source of a tri-gate quantum-wire MOSFET device with $V_g = 0.35$ V and $V_d = 0.1$ V.

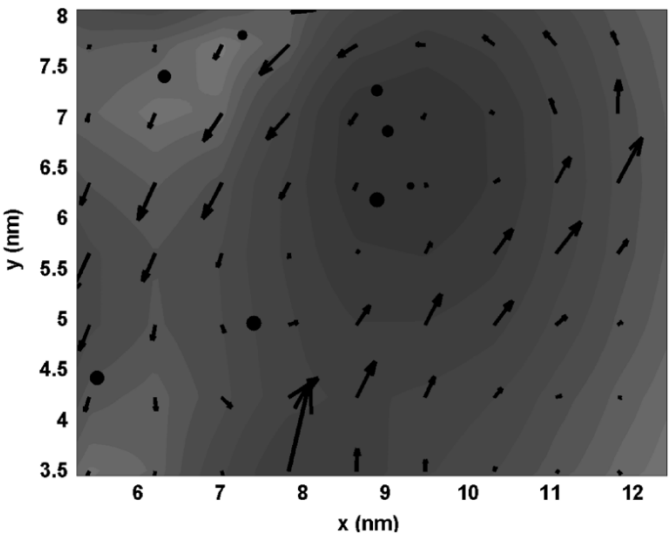

Fig. 8. Close-up of the vortex formed in bottom of the source of a tri-gate quantum-wire MOSFET device with $V_g = 0.35$ V and $V_d = 0.1$ V.

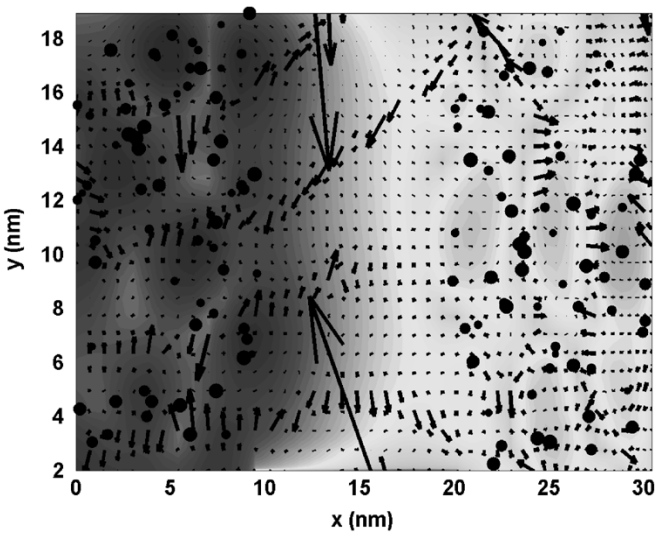

Fig. 9. Electron density at a depth of 7 nm into a tri-gate quantum-wire MOSFET device with $V_g = 0.10$ V and $V_d = 0.25$ V.

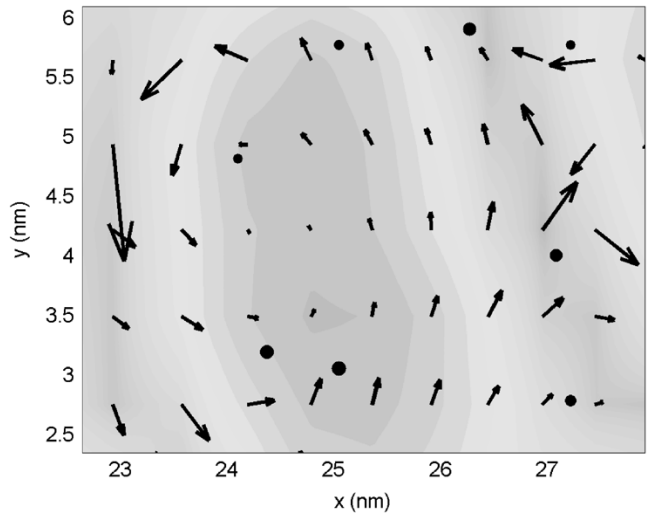

Fig. 10. Close-up of the vortex formed in the source of a tri-gate quantum-wire MOSFET device with $V_g = 0.10$ V and $V_d = 0.25$ V.

While it is clear that the vortices appear at preferential locations in the source and drain as the gate voltage is swept, we now consider if the vortices appear at an elevated drain voltage. In Fig. 9, we plot the electron density for the positive propagating electrons at a drain voltage of $V_d = 0.25$ V. The elevated electric field in the channel and drain keeps the density from forming vortices in the drain. A vortex does form in the source of the device, shown in Fig. 10. This is quite simple to understand as the electrons in the source have not yet been accelerated by the applied voltages and, therefore, become trapped in the potential corrals.

IV. Results for the Quasi-Ballistic Regime

A. I–V Characteristics

In Fig. 11(a), we plot the I_d–V_g curves corresponding to the four devices previously shown in Fig. 2(a) with the dissipation added. For the quasi-ballistic simulations, we assume τ_ϕ of 1.1 ps. Clearly, the quantum interference present in Fig. 2(a) has been significantly reduced by the scattering, producing an almost routine sweep of the gate voltage. The addition of the scattering to the calculation has the affect of lowering the overall energy of the carriers as they impinge on the source–channel barrier. Therefore, their interaction with the barrier is as intense as the ballistic case. The lower energy carriers then have more difficulty populating the channel where they are then accelerated by the gate and drain voltages. This channel depopulation lowers the magnitude of the reflections at the channel–drain interface as well. The overall consequence is a reduced transmission. This is further confirmed in Fig. 11(b). For $V_g = 0.1$ V, the currents are smooth up to approximately $V_d = 0.1$ V. After this voltage, the acceleration that the carriers undergo in the channel begins to overwhelm the effects of the scattering and the peaks begin to again show up. However, for this gate voltage, the channel is just becoming conducting and the large reflections by the source–channel barrier keep the channel rather sparsely populated. A much better illustration of

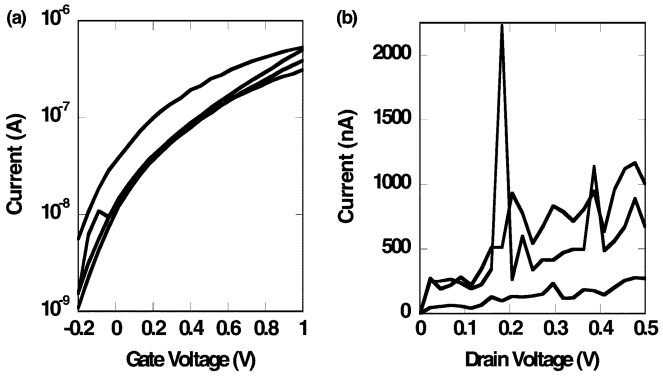

Fig. 11. (a) I_d–V_g plot for the same four devices that were shown in Fig. 2(a) with dissipation now included. (b) I_d–V_d curves for the same device as in Fig. 2(b) with scattering included in the simulation. From bottom to top, the gate voltages are 0.1, 0.7, and 1.0 V.

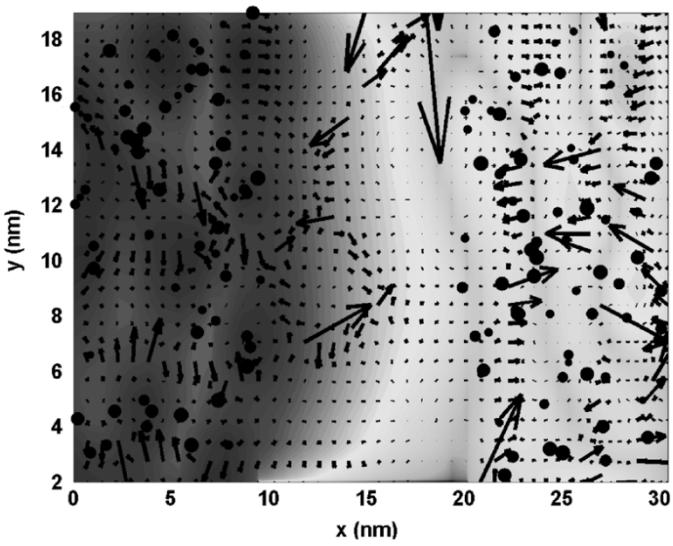

Fig. 12. Electron density at a depth of 7 nm into a tri-gate quantum-wire MOSFET device with $V_g = -0.05$ V and $V_d = 0.1$ V with dissipation included.

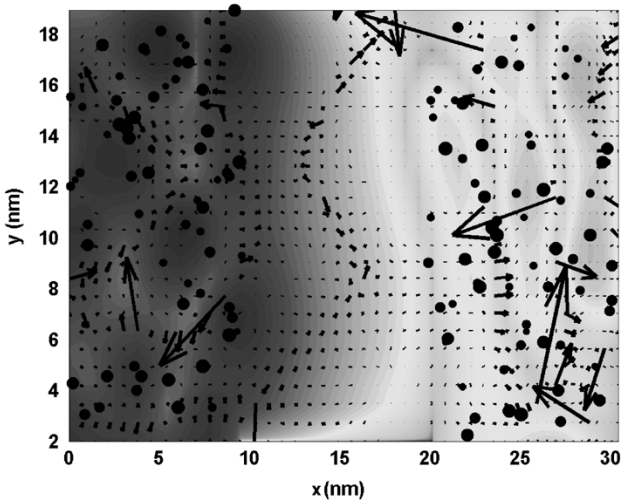

Fig. 13. Electron density at a depth of 7 nm into a tri-gate quantum-wire MOSFET device with $V_g = 0.35$ V and $V_d = 0.1$ V with dissipation included.

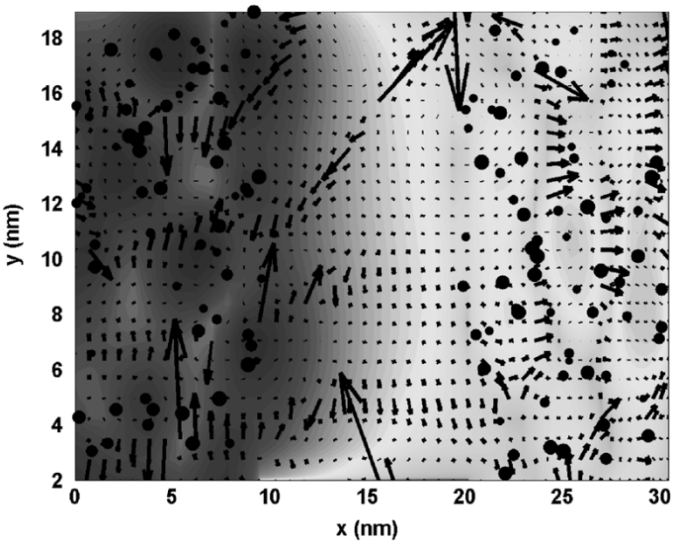

Fig. 14. Electron density at a depth of 7 nm into a tri-gate quantum-wire MOSFET device with $V_g = 0.10$ V and $V_d = 0.25$ V with dissipation included.

the carriers overcoming the dissipation is seen when $V_g = 1$ V. Here, the channel is fully populated, as we are well above threshold. Even with the dissipation, the carriers undergo such a large acceleration that large peaks, of equal magnitude to the ballistic case, are seen before the bias reaches $V_d = 0.2$ V. It is important to note that the introduction of scattering has *not* overcome the variation in the threshold voltage with different dopant configurations in the source and drain. The average threshold voltage is 0.138 V, but has a statistical variance of 0.009 V when averaged over ten devices. This is a only a small improvement over the ballistic case in the spread of the threshold voltages without a significant reduction in the output current.

B. Electron Density

We now examine the electron density at the same gate voltages of the previous section to determine the stability of the vortices seen in the ballistic case. In Fig. 12, we plot the electron density at $V_g = -0.05$ V. In the ballistic case, we found vortices in both the source and drain of the device. Here, we see that the lower energies caused by the dissipation keep the electrons from being trapped in the ring of potential formed by the dopant ions in certain cases. Further, the channel is less populated than in the ballistic case, as mentioned in Section IV-A.

In Fig. 13, we plot the electron density for $V_g = 0.35$ V. Obviously, the channel is more populated than in Fig. 10 from the increase in the gate voltage, but we also see that there is a distinct separation between the channel and drain at the interface. The density no longer has sufficient energy to easily reach the drain and, therefore, more of the density is reflected at the interface creating a density dip at the channel–drain interface. The dissipation washes out the vortices in the source of the device and we are left with only weak circulation. In Fig. 14, we raise the drain voltage. Once again, the change in the carrier energy washes out the vortex that was formed in the drain in Fig. 9.

V. Conclusion

These results outline the impact of quantum interference in tri-gate quantum-wire MOSFETs and how they change with the addition of inelastic scattering. The formation of vortices arises from formation of a ring of preferential sites in the source and drain in which the velocity vector circulates. Resonances are seen in the output currents due to the interaction of the density with the dopant ions and reflections from the different regions of the device. When inelastic scattering is included, we find that the vortices are washed out regardless of the drain or gate voltage. We also conclude that the peaks in the current are washed out for low drain voltages due to the decreased energy of the carriers. We find that the peaks return when the drain voltage is increased, giving the carriers sufficient energy to overcome the dissipation. Finally, we find that the dissipation seems to stabilize the variation in threshold voltage variation without a significant decrease in the output current.

In summary, we have used a full 3-D quantum mechanical simulation approach to study the dynamics of current flow in tri-gate SOI quantum-wire MOSFETs both in the ballistic and quasi-ballistic regime. Scattering was introduced to the Hamiltonian through a generic imaginary term to study the quasi-ballistic transport. This is an effective method to study the basic effects of scattering; better options are available and will be discussed in a future paper.

References

[1] H. S. Doyle, S. Datta, M. Doczy, S. Hareland, B. Jin, J. Kavalieros, T. Linton, A. Murthy, R. Rios, and R. Chau, "High performance fully depleted tri-gate CMOS transistors," *IEEE Electron Devices Lett.*, vol. 24, no. 4, pp. 263–265, Apr. 2003.

[2] H. Namatsu, K. Kurihara, M. Nagase, and T. Makino, "Fabrication of 2 nm wide silicon quantum wires through a combination of partially shifted resist pattern and orientation-dependent etching," *Appl. Phys. Lett.*, vol. 70, pp. 619–621, 1997.

[3] M. J. Gilbert and D. K. Ferry, "Efficient quantum 3-D modeling of fully depleted ballistic SOI MOSFETs," *J. Appl. Phys.*, vol. 95, pp. 7954–7962, 2003.

[4] R. Akis, J. P. Bird, and D. K. Ferry, "The effects of inelastic scattering in open quantum dots: Reduction of conductance fluctuations and disruption of wave-function scarring," *J. Phys, Cond Matt.*, vol. 8, pp. L667–L674, 1996.

[5] M. J. Gilbert and D. K. Ferry, "Discrete dopant effects in ultra-small fully depleted ballistic SOI MOSFETs," *Supperlatt. Microstruct.*, vol. 34, pp. 277–282, 2003.

[6] ——, "Vorticity and quantum interference in ultra-small SOI MOSFETs," *IEEE Trans. Nanotechnol*, vol. 4, no. 3, pp. 355–359, May 2005.

[7] S. E. Laux, A. Kumar, and M. V. Fischetti, "Analysis of quantum ballistic electron transport in ultrasmall silicon devices including space-charge and geometric effects," *J. Appl. Phys.*, vol. 95, pp. 5545–5582, 2004.

Matthew J. Gilbert (S'98), photograph and biography not available at time of publication.

David K. Ferry (S'61–M'62–SM'72–F'87), photograph and biography not available at time of publication.